Low-energy structure of ^{40}S through ^{40}P β decay

J. A. Winger
Department of Physics and Astronomy, Mississippi State University, Mississippi State, Mississippi 39762-5167

P. F. Mantica
Department of Chemistry and National Superconducting Cyclotron Laboratory, Michigan State University, East Lansing, Michigan 48824

R. M. Ronningen
National Superconducting Cyclotron Laboratory, Michigan State University, East Lansing, Michigan 48824

M. A. Caprio
A. W. Wright Nuclear Structure Laboratory and Department of Physics, Yale University, New Haven, Connecticut 06520
(Received 4 June 2001; published 20 November 2001)

Results from the study of the β decay of ^{40}P, produced in the fragmentation of a ^{48}Ca beam, are presented. The ^{40}P half-life and delayed-neutron emission probability have been measured to be 153 ± 8 ms and $15.8\pm2.1\%$, respectively. On the basis of γ-ray singles and $\gamma\gamma$ coincidence data, 21 γ rays have been assigned to the decay. Three γ rays are assigned to excited states in ^{39}S populated in the delayed-neutron branch while a total of 15 γ rays were placed in a level scheme for ^{40}S with nine excited states up to 5 MeV. The structure of low-energy states in ^{40}S has been fit using the geometrical collective model that indicates the structure to be consistent with that of an anharmonic oscillator with a soft potential.

DOI: 10.1103/PhysRevC.64.064318 PACS number(s): 21.10.−k, 21.60.Ev, 23.40.−s, 27.40.+z

I. INTRODUCTION

A major question in nuclear structure physics is the degree to which the magic numbers observed near stability continue to be valid further from stability. Although numerous experiments have shown the doubly magic nature of ^{132}Sn, experiments have also identified a region of deformed nuclei near the supposedly singly magic nucleus ^{32}Mg. This failure of the magic numbers is further supported by the apparent particle instability of the doubly magic nucleus ^{28}O [1,2]. This paper presents results of an experiment to study low-energy nuclear structure in the region near the potentially singly magic nucleus ^{44}S. Both experimental and theoretical analyses of this region suggest a weakness in the strength of the $N=28$ shell closure.

The possibility of deformation in the ^{44}S region was first presented by Möller and Nix [3]. More recently, Werner *et al.* [4,5] performed calculations indicating the possibility of deformation near ^{44}S. At about the same time, Sorlin *et al.* measured the decay half-life and β-delayed neutron emission probability for ^{43}P, ^{42,44,45}S, $^{44-47}$Cl, and ^{47}Ar [6,7]. Spurred by these results, several experimental studies to search for evidence of deformation in this region have been performed. In particular, the 2_1^+ energies and the $B(E2,0^+_{\text{g.s.}}\rightarrow 2_1^+)$ values have been measured for several neutron-rich silicon, sulfur,and argon nuclei using intermediate-energy Coulomb excitation [8–12]. The systematic trends in the $|\beta_2|$ (quadrupole deformation parameter) values extracted from these experiments for even-even sulfur and argon nuclei indicate a trend toward collective behavior,and possibly deformed shapes, for both the argon and sulfur isotopes near mid shell ($N=24,26$). For singly magic $N=28$ nuclei, ^{46}Ar exhibits a much smaller $B(E2,0^+_{\text{g.s.}}\rightarrow 2_1^+)$ value indicating a less collective behavior while for ^{44}S the $B(E2,0^+_{\text{g.s.}}\rightarrow 2_1^+)$ value remains relatively high ($314\pm88\ e^2\text{fm}^4$) suggesting weakness in the $N=28$ shell closure [8,9]. Bernstein, Brown, and Madsen [13] have shown that the hadron scattering transition multipole matrix elements may be written as a linear combination of proton and neutron multipole matrix elements. The coefficients b_p and b_n are the external field proton and neutron multipole field strengths. For proton scattering at 10–50 MeV, the ratio $[b_n/b_p]$ is approximately 3, and then tends towards unity at much higher energies (near 1 GeV). Therefore, low-energy proton scattering is quite sensitive to the neutron distribution and, therefore, the neutron deformation. Kelley *et al.* [14], Maréchal *et al.* [15,16], and Scheit *et al.* [17] have performed proton scattering experiments in inverse kinematics for the radioactive isotopes ^{38,40}S and ^{42,43,44}Ar. Their results indicate that the 2_1^+ states in these nuclides have a strong neutron contribution with a larger deformation than was observed in the Coulomb excitation measurements. Although these experiments provide information on collectivity, they can neither determine the ground-state shape nor distinguish between static deformation or vibrational collectivity. Therefore, complementary experiments are needed to provide additional nuclear structure information. Presented here are the results from the measurement of the β decay of ^{40}P into excited states of ^{40}S.

The β decay of ^{40}S was first studied at GANIL using fragmentation of a ^{40}Ar beam in the LISE spectrometer [18]. The ^{40}S ions were stopped and their decay observed with a plastic scintillator and a single Ge detector. The decay half-life was measured to be 8.8 ± 2.2 s and four γ rays were associated with the decay. In a similar experiment, fragmentation of a ^{48}Ca beam was used to produce and study β-delayed neutron emission from ^{40}P using a $4\pi\beta$-n coin-

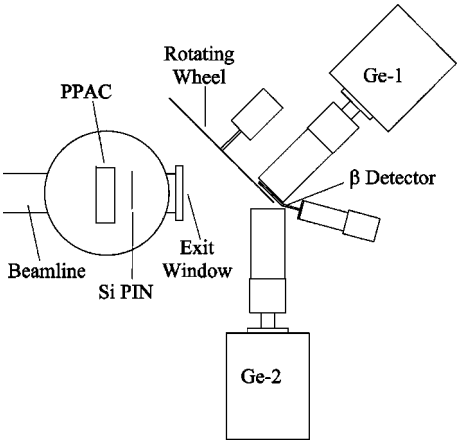

FIG. 1. Schematic layout of the detector endstation including detectors for particle identification and tracking, a rotating wheel into which the radioactive beam was implanted, and detectors for observing the β decay.

cidence detector [19]. The measured values for the half-life and delayed-neutron probability were 260^{+100}_{-60} ms and 30 $\pm 10\%$, respectively.

II. EXPERIMENTAL PROCEDURE

Sources of ^{40}P were produced via fragmentation of 70 MeV/nucleon ^{48}Ca beam in the A1200 fragment separator of the National Superconducting Cyclotron Laboratory at Michigan State University [20]. The ^{48}Ca primary beam was produced in a room-temperature ECR ion source using metallic feeding and accelerated through the K1200 cyclotron resulting in beam intensities ranging from 2 to 5 pnA [21]. The ^{40}P fragments were produced in a 254 mg/cm^2 Be target and identified using standard energy loss versus time of flight techniques. By scanning the A1200 in rigidity, peak production of the ^{40}P fragments was observed at $B\rho = 2.9073$ T m. A 3% momentum slit was used at the first intermediate image of the A1200 to make the initial selection of fragment ions. Further separation of the fragment ions was obtained by use of a thin plastic wedge placed at the second intermediate image of the A1200. After passing through the wedge, the ^{40}P ions were centered at the focal plane of the A1200 by tuning the second half of the device to a rigidity of 2.5316 T m. These ions were then transported to a detector endstation located approximately 40 m downstream from the A1200. The transport efficiency of the beam line was $\approx 65\%$ that resulted in an average beam intensity of ≈ 38 ions per second of ^{40}P at the detector endstation.

The detector endstation used in this experiment is shown schematically in Fig. 1. Identification of the ions transported to this location was obtained using a Si PIN diode near the beam-line exit for energy loss determination with the time-of-flight measurement being made relative to a thin plastic detector placed just downstream from the A1200 exit. These detectors allowed precise determination of the components of the beam and a parallel-plate avalanche counter (PPAC) was used to monitor the beam position. Events associated with the beam were flagged and recorded. These events were not correlated to the events associated with β decay, but did provide overall information on the composition of the beam during the experiment. The ions exited the beam line through a 0.13 mm Kapton window that was followed by a layer of Al foil for slowing the ions, and were then imbedded into 117 mg/cm Al targets attached to a rotating wheel. The final beam spot size on the catcher foils was less than 1 cm. With the settings optimized for production and transport of ^{40}P, the final separated beam had a purity of $\approx 45\%$. The two primary contaminants in the beam were ^{43}Cl ($\approx 42\%$) and ^{42}S ($\approx 8\%$). The presence of these contaminants in the beam complicated the analysis since multiple decay chains were observed. This was especially true in this case where both ^{42}S and ^{43}Cl had not been studied previously. However, this also provided the opportunity to simultaneously study the decay of these two nuclides.

The rotating wheel into which the separated ions were implanted consisted of a 40 cm diameter wheel attached to a stepping motor with the wheel oriented at 45° to the direction of the beam. The wheel was made from a $\frac{1}{8}$-in-thick Al plate having nine 5 cm diameter holes covered with 117 mg/cm Al foils at a radius of 17.2 cm. This provided an effective stopping thickness of ≈ 165 mg/cm^2 for the beam ions, and was sufficient to handle the expected range straggling associated with the full 3% momentum acceptance of the A1200. Thin catcher foils were used in order to minimize the material through which β particles from the decays would need to penetrate before reaching the detectors. The wheel could be stepped between adjacent target positions in approximately 300 ms. A typical timing cycle would consist of a period of implantation during which data were taken, a period for observation of the decay only, and finally a 300 ms period while the wheel was moved and no data were collected. During the second and third time periods, the beam was stopped by dephasing one dee of the cyclotron. To minimize the possibility of γ rays from catcher foils other than the one at the beam position from reaching the Ge detectors, the front and back sides of the wheel were shielded by a $\frac{3}{8}$-in-thick steel plate.

The decays of the implanted ions were observed using three detectors, two Ge detectors and one thin plastic scintillator. The β detector consisted of a 1 mm thick by 6.3 cm diameter BC400 plastic scintillator that was attached to a photomultiplier tube by a short lightguide. The 1-mm-thick plastic is $\sim 100\%$ efficient in detecting β particles and almost transparent to γ rays. This conclusion is supported by observing that the measured γ-ray intensities for both detectors were consistent, indicating that events due to a single γ ray triggering both the β detector and Ge-1 (see Fig. 1) were negligible. Again in order to minimize the material through which the β particles must penetrate to reach the detector, the face of the scintillator toward the implantation target was covered with a thin Al foil. An 80% efficient Ge detector, labeled Ge-1 in Fig. 1, was located just behind the β detector, with both being oriented at 45° relative to the beam direction. A 120% Ge detector, labeled Ge-2 in Fig. 1, was placed at 90° relative to the beam direction. The average distances from the implantation targets to the two Ge detectors were 1.8 cm and 4.1 cm, respectively. The Ge crystals

were shielded by a 2.5-cm-thick Pb box to reduce background radiation from the room, but the orientation of the two detectors resulted in significant backscattering between the detectors. Timing signals from the three detectors were used to set hardware timing gates. Data from the detectors were only collected when two of the detectors were in coincidence based on these timing gates. Further refinement of these gates was performed by use of software gates during off-line analysis. In this way, data on $\beta\gamma$, $\gamma\gamma$, and $\beta\gamma\gamma$ coincidences were obtained. In addition to energy and relative times, the time of each event relative to the beginning of a decay cycle was recorded. The clock for this measurement was reset at the end of each cycle and not restarted until the start of the next decay cycle so that during the growth phase of the timing cycle events did not have a time recorded.

Energy calibration of the Ge detectors was performed off-line using standard sources of ^{60}Co, ^{88}Y, ^{152}Eu, and ^{207}Bi, and on-line using both background lines as well as lines from the decays. This was necessary since the standard calibration sources only provided a useful energy calibration between 100 keV and 2.7 MeV, while γ rays were observed with energies up to 4.1 MeV. In order to obtain a single consistent energy calibration, a multiple step process was used. First, the energy calibration was performed for both detectors over the range from 100 keV and 2.7 MeV using the standard sources. For this measurement, the souces were placed at a distance from the detectors so that the detection rate was less than 1000 cps to limit any rate related gain shifts. Second, this calibration was used to determine the energies of background and/or long-lived lines due to Pb x rays, $\beta+$ annihilation, ^{40}K, and ^{40}Cl in order to test the calibration and check for gain shifts between the calibration measurements and during the run. All gain shifts were small and have been considered in the calibration process. Third, single and double escape peaks from the on-line radioactive sources were used to ''bootstrap'' the calibration up to higher energies. At each step, the average of the γ-ray energies from each detector was used. Finally, the full set of calibration, background, and on-line γ-ray energies was used to fit a fifth-order polynomial that was used as the final calibration. γ-ray energies presented here are based on this calibration with the uncertainties based on both measured uncertainties in the position of the γ-ray peaks in the spectra as well as variance and covariance effects associated with the calibration.

Efficiency calibrations for the Ge detectors were performed using calibrated ^{60}Co, ^{88}Y, and ^{152}Eu sources placed at the implantation point of the radioactive beam. Due to the small detector distance, coincidence summing effects were significant. Making these corrections required determination of both the absolute photopeak and total efficiencies of the two detectors. The ratio between absolute and total efficiencies was measured separately using ^{22}Na, ^{54}Mn, ^{57}Co, ^{60}Co, ^{109}Cd, ^{137}Cs, and ^{241}Am sources at distances ranging from 1.5 to 7.5 cm. This information was then used to estimate the total efficiency curve for each detector at the appropriate detector to source distance. (A precise determination of the total efficiency curve is not needed since the summing effects are secondary in that a large uncertainty in the total efficiency curve does not create a correspondingly high uncertainty in the absolute photopeak efficiency curve.) Once a corrected set of absolute photopeak efficiencies was obtained, a curve was fit to the data points. As with the energy calibration, the need to extrapolate the curve to higher energies required additional care. If plotted on a log-log plot the efficiency curve over the range from 300 keV to 3 MeV is linear with photon energy [22]. However, a detailed study of Ge detector efficiency indicates that the efficiency for energies above 3 MeV begins to fall off slightly while the curve peaks between 100 and 200 keV before falling off rapidly at low energies [23,24]. To account for this trend, it was noted that the basic shape of the efficiency curve for our detectors and the detector studied by Kis *et al.* were nearly the same with the primary difference being a shift in absolute scale. Estimated values for the efficiency over the range from 3 to 7 MeV based on the work of Kis *et al.* were then included and a fifth-order polynomial function on a log-log scale was used to obtain the final calibration curve. The uncertainty in the final efficiency curve ranges from about 2% for energies in the range from 0.5 to 1.5 MeV and then increases to 6% at 4 MeV. For energies below 400 keV, the turn over of the efficiency curve resulted in uncertainties that increase from 3% at 300 keV to 8% at 100 keV.

III. EXPERIMENTAL RESULTS

A. Decay of ^{40}P

The presence of strong contaminants from ^{43}Cl and ^{42}S, as well as daughter nuclei from these decays, required the use of several timing cycles and A1200 settings in order to positively associate specific γ rays with their radioactive source. With the magnetic rigidity of the A1200 set for maximum transmitted yield of ^{40}P, data were collected using three different timing cycles. The choice of these timing cycles was based on the previously reported half-life of ^{40}P ($T_{1/2}=260^{+100}_{-60}$ ms) [19]. With a timing cycle of 500 ms growth with 1000 ms decay (long cycle), data were collected for a total of 4 hours in order to obtain a more precise half-life value. The second timing cycle used 500 ms growth with 500 ms decay (short cycle) in order to enhance the events from ^{40}P decay relative to those from other decays. Data were collected with this timing cycle for a total of 17 hours. Finally, data were collected during two saturation measurements, one at the beginning and the other at the end of the experiment. For these measurements, the beam was implanted into a single catcher for a period of five minutes before data were collected for periods of 40 and 35 minutes, respectively. This insured that the $A=40$ decay chain was in saturation and that at least ^{39}S was in saturation in the $A=39$ decay chain. The implantation rate for ^{40}P averaged $\sim$38 ions/second during the beam on periods resulting in a total of $\sim 10^6$ ions being implanted. Additional A1200 settings and timing cycles were used to enhance the separation and observation of both ^{43}Cl and ^{42}S in order to better study these decay chains.

β-gated γ-ray energy spectra for each setting of the system (A1200 setting plus timing cycle) were generated from the event data and fit to provide a complete set of all ob-

TABLE I. γ rays observed in ^{40}P decay.

E_γ (keV)	I_γ[a,b,c]	Placement	Coincident γ rays (keV)[d]
339.88±0.11	4.6±0.5	^{40}Pβn	465
398.61±0.14	6.1±0.9	^{40}P βn	465
465.45±0.19	4.5±0.9	^{40}P βn	339, 398
648.82±0.15	5.7±0.5	4138−3489	3489
834.90±0.08	5.7±1.7		
903.68±0.09	100±2	903−0	981, 1013, 1351, 2469, 2585, 2808, 3043, 3234, 4105
981.2±0.4	2.5±0.4	3236−2254	903, 1351
1013.17±0.20	5.2±1.2	1916−903	903
1351.10±0.14	12.5±0.9	2254−903	903, 981, 2469
1692.6±0.9	1.1±0.4	3947−2254	(903), 1351
1773.2±0.7	1.4±0.4	5009−3236	(903), (1351)
2254.5±0.9	0.2±0.3	2254−0	
2469.79±0.20	6.4±0.9	4724−2254	903, 1351
2550.4±0.5	1.7±0.4		903
2585.6±0.4	3.2±0.6	3489−903	903
2614.8±0.3	2.6±0.9		
2808.2±0.9	5.5±1.5	4724−1916	903
3043.2±0.4	4.4±0.5	3947−903	903
3234.7±0.4	41.5±2.9	4138−903	903
3489.6±0.4	24.9±2.4	3489−0	648
4105.7±0.4	16.5±2.3	5009−903	903

[a]Normalized to 100 for the intensity of the 903-keV γ ray. See text.
[b]Corrected for coincidence summing effects. See text.
[c]Multiply by 0.63±0.03 to obtain absolute intensities.
[d]Possible coincidence relationships are indicated in parentheses.

served γ rays. Detailed comparisons between these sets allowed the observed γ rays to be associated with particular decays. Additional information was provided by coincidence relationships. Based on this information, a total of 21γ rays, excluding single and double escape peaks, were associated with the decay of ^{40}P. The strongest γ ray associated with the decay of ^{40}P was observed at 903 keV and corresponds to the energy of the first excited state in ^{40}S in agreement with Scheit *et al.* [8]. Those γ rays that could not be associated with a particular decay had relative intensities to the 903-keV γ ray of less than 2%. Table I contains information on the measured γ-ray energies and intensities, placements, and coincidence relationships. The energies and intensities presented are based on weighted averages from the various data sets. The intensities quoted also include corrections due to coincidence summing that is based on the proposed level scheme. A β-gated γ-ray singles spectrum for Ge-2 is presented in Fig. 2.

Background-subtracted coincidence γ-ray spectra were obtained using standard techniques. These coincidence spectra were gain shifted to one channel per keV. Fig. 3 shows the coincidence spectra gated on the 903- and 1351-keV γ rays, respectively. The energies of the coincident γ rays are indicated in the spectra. The large number of counts at low energy in the 903-keV gated spectrum are due to Compton scattering between the two detectors that severely limited the search for weak transitions in the low-energy portion of the spectrum.

Based on the γ-ray singles and coincidence information, 15 γ rays were placed in the decay scheme for ^{40}P that populate nine excited states in ^{40}S. Details of this decay scheme, which is shown in Fig. 4, will be presented in the following sections. Three γ rays (339, 398, and 465 keV) were assigned to excited states in ^{39}S populated following β delayed-neutron decay of ^{40}P. This was confirmed in a subsequent experiment that observed the β decay of ^{39}P [25]. Three γ rays associated with this decay remain unplaced due to lack of coincidence and energy sum relationships.

B. Half-life of ^{40}P

The half-life of ^{40}P was determined using a time spectrum gated by the 903-keV γ ray. Since this method would also project out the time of any background events within the gate, a background gated time spectrum was also projected. The background gate was placed at an energy slightly higher than the peak gate since there were no γ rays in this region, and the width of the gate matched that of the peak gate. This procedure was performed for both the short and long timing cycles. The four spectra obtained in this procedure are displayed in Fig. 5. In fitting these time spectra, the background was determined for each timing cycle and then held fixed when fitting the data for the half-life.

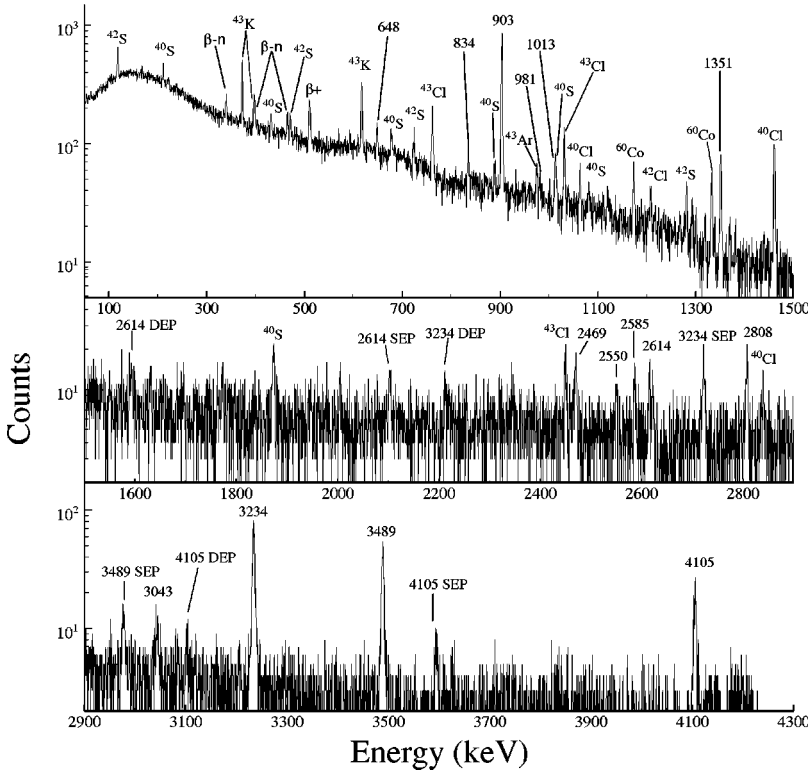

FIG. 2. β-gated γ-ray singles spectrum from Ge-2 with the A1200 set to maximize the transmitted intensity of ^{40}P to the detector endstation. The spectrum includes data from both the long and short timing cycles. Lines assigned to the decay of ^{40}P are labeled with their energy in keV. Single escape peaks (SEP) and double escape peaks (DEP) are labeled with the energy of the original γ ray followed by SEP or DEP, respectively. Three lines associated with the β-delayed neutron branch to states in ^{39}S are indicated by β-n. All other lines are labeled according to their source.

The background time spectrum for the long cycle can be easily characterized by a single constant value. By fixing the value for the background in the fit of the decay time spectra, a half-life value of 153 ± 14 ms was obtained. The quoted uncertainty represents the maximum range of values obtained by using the 1σ extremes for the background value while the half-life value comes by using the best value for the background. The background data for the short cycle

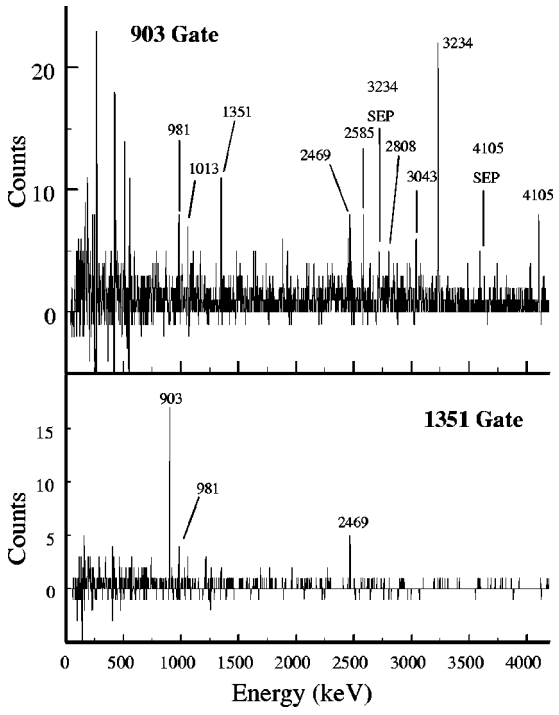

FIG. 3. Background-subtracted γ ray coincidence spectra gated on the 903- and 1351-keV γ rays. Labels indicate the energy of coincident γ rays in keV.

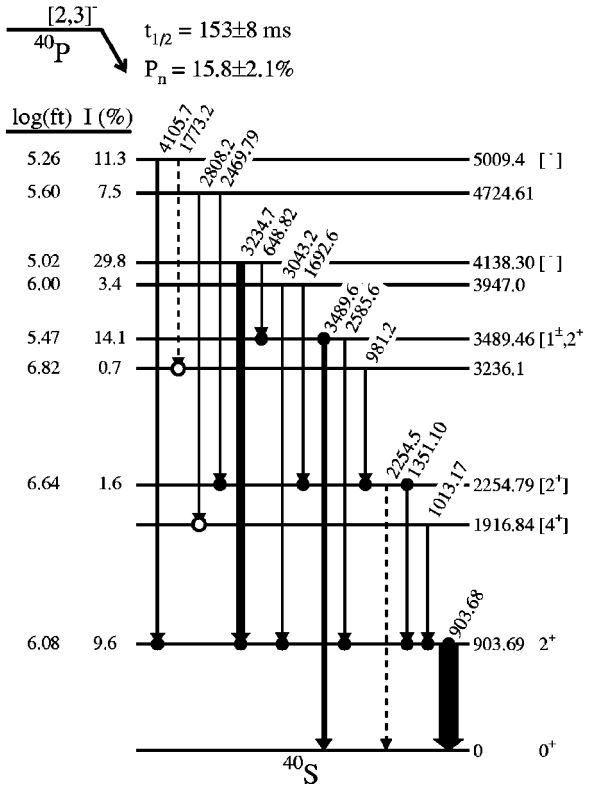

FIG. 4. Level scheme for ^{40}S. The width of the lines is proportional to the relative intensity of the γ ray.

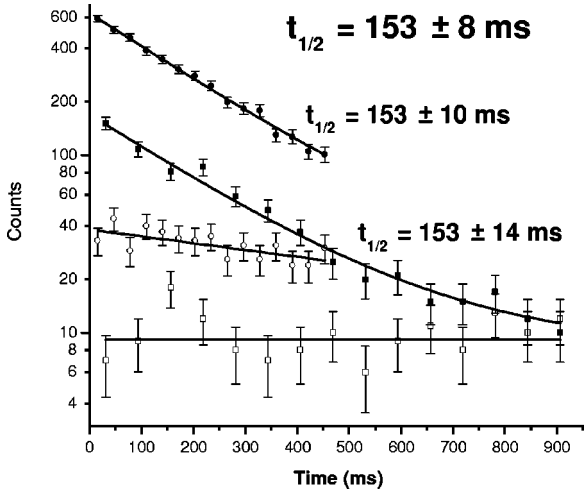

FIG. 5. Half-life curve for the decay of the 903-keV γ ray associated with ^{40}P β decay. In the figure, circles represent data from the short timing cycle and squares the long timing cycle, where closed(open) symbols represent the time spectrum projected by gating on the γ-ray peak(background). A best fit to each data set, describe in the text, is shown as solid lines.

indicates a slight decay, therefore, it was fit as a single decaying exponential instead of as a constant. This decaying background is due to a composite of longer lived components of the beam with half-lives in the range of hundreds of milliseconds to several seconds that contribute to the overall Compton background. The resulting ''half-life'' for the background was 0.79 ± 0.31 s. Using this information, the decay timing spectrum was fit using two decaying exponential functions where the parameters for the background were held fixed. Again, the full range of the background parameters were used in order to obtain a better estimate of the uncertainty in the final value for the half-life. By this method, a measured half-life of 153 ± 10 ms was obtained. The better accuracy in this second measurement is a result of the higher statistics where a significant fraction of the uncertainty is related to the range of uncertainty in the background parameters. A weighted average of the results from the two cycles was then used to obtain the final result of 153 ± 8 ms.

Lewitowicz *et al.* [19] obtained a half-life for ^{40}P of 260^{+100}_{-60} ms by observing the β-delayed neutrons from ^{40}P. Our result differs by almost 2σ, but it is also much more precise and the gate on the 903-keV γ ray guarantees the correct identification of the parent. A comparison of our measured half-life to that of several model calculations is presented in Table II. The estimates based on the gross theory of β decay significantly overestimate the experimental result [26,27]. In contrast, an early microscopic calculation significantly underestimated the experimental result [28]. However, the more recent microscopic calculations show excellent agreement with the measured value [29,30].

C. β-delayed neutron emission

The large Q_β value for ^{40}P (14.5 MeV) [31] and the one- and two-neutron separation energies in ^{40}S (7.7 and 12.2 MeV, respectively) [30] provide a large energy window for

TABLE II. Comparison of measured half-life for ^{40}P β decay to model calculations.

$t_{1/2}$ (ms)	Reference
153 ± 8	Present work
283	Takahashi, Yamada, and Kondoh [26]
376	Nakata, Tachibana, and Yamada [27]
18	Klapdor, Metzinger, and Oda [28]
160	Staudt *et al.* [29]
134	Möller, Nix, and Kratz [30]

β-delayed one- and two-neutron emission. Lewitowicz *et al.* measured the neutron emission probability (P_n) for ^{40}P to be $30\pm10\%$ by direct observation of the emitted neutrons [19]. We have remeasured the delayed-neutron emission probability by comparing the intensities of γ rays in the $A=39$ and 40 mass chains. This is possible since ^{40}P is the only member of the $A=40$ mass chain and no members of the $A=39$ or lighter mass chains were present in the separated beam.

The method used in this determination requires the absolute branching ratios for β decay for some member of each decay chain. First, the relative intensity for a subset of γ rays from each of the decay branches is determined. For clarity, the decay branches will be labeled β, 1n, 2n, etc. Second, dividing the relative intensity by the known branching ratio for each γ ray provides a number (f_β, f_{1n}, f_{2n}, etc.) that is the same for all γ rays within the branch (i.e., each mass chain). This allows a weighted average based on all the transitions for each decay path to be used. Although the branching ratios used are based on decay only within the branch, they provide information on the relative branching of the original decay into each branch. Finally, by taking ratios one obtains numbers that are independent of the absolute branching ratio. In general, the probability of decay through the β branch is given by

$$P_\beta=\frac{1}{1+\sum\frac{f_{in}}{f_\beta}}.$$

With this value known, it is then possible to obtain the probability for each of the other branches by multiplying by the ratio of ''f'' numbers. In the case where only the one-neutron branch is observed, P_{1n} can be found directly from

$$P_{1n}=\frac{1}{1+\frac{f_\beta}{f_{1n}}}.$$

Our measurement was based on the relative intensities of γ rays from ^{39}S (1300 and 1696 keV) [32] and ^{40}Cl (1460, 2839, and 3101 keV) [33]. It was necessary to use the two higher energy γ rays from ^{40}Cl decay in order to check for possible contamination of the 1460-keV line from background ^{40}K. The consistency of the results for the three ^{40}Cl γ rays indicates that background contamination from ^{40}K was negligible. The decay of ^{39}Cl was not considered, even

though the branching ratios are better known, since it was not in saturation while the data were collected. The possibility of a two-neutron branch was also considered, but no γ rays from the $A=38$ mass chain were observed. However, this is not a conclusive result since the half-lives of ^{38}S (170.3 m) and ^{38}Cl (37.24 m) are long in comparison to the data collection time so that they were not in saturation and probably would not be seen even if a weak branch were present. Assuming only the one-neutron branch was present, we obtained a delayed-neutron emission probability of 15.8 $\pm$2.1%. This result is significantly lower than that obtained by Lewitowicz *et al.*, but is in close agreement with the predicted value of 14% given by Möller, Nix, and Kratz [19,30]. Note that the values of P_{1n} and P_β determined using this method are independent of any knowledge of the ^{40}P decay. In addition, the predicted probability for the two-neutron branch is only 2% that is within the limits of our uncertainty. Hence, any unobserved intensity to the two-neutron branch would have only a minor effect on our result.

D. ^{40}P ground state

The ground-state spin and parity of ^{40}P can be estimated based on theoretical arguments coupled with some experimental results. From simple shell model considerations, the ground state of odd-odd ^{40}P should come from the coupling of single nucleons in the $\pi s_{1/2}$ and $\nu f_{7/2}$ resulting in possible states of $(3,4)^-$. Möller, Nix, and Kratz suggest that, based on prolate deformation, the ^{40}P ground state will involve the coupling of the $\pi 1/2[211]$ and the $\nu 5/2[312]$ Nilsson orbitals resulting in possible states of $(2,3)^-$ [30]. Furthermore, even with large deformation, the proton will occupy an even parity state while the neutron occupies an odd parity state. Based on this information, one would expect little feeding in the decay to the ground state of ^{40}S and that the ^{40}P ground state has odd parity.

Since ^{40}P was the only member of the $A=40$ mass chain separated in this experiment, it is possible to directly estimate the ground-state feeding for its decay from a saturation spectrum. The objective is to identify any missing decay strength, similar to the method outlined for the delayed-neutron probability. Since all γ decays within the β branch have the same "f" value, one only needs to use this value to relate a known branching ratio within the decay chain to the intensity of the 903-keV transition. Based on the known decay branches for ^{40}Cl, the feeding of the 903-keV γ ray was measured to be 63$\pm$3% where the β branch probability ($P_\beta=84.2\pm2.1\%$) has been included. Using this factor, the absolute feeding for all the observed γ rays was determined and the feeding to the levels was calculated. (See Table III.) From this, it was possible to determine that only 6$\pm$5% of the total β decay strength was not observed.

Two possibilities exist to explain the missing strength. The first is that this represents direct feeding to the ground state of ^{40}S. However, the theoretical arguments already presented point away from this conclusion. A lower limit for the log(ft) value of 6.2 is found by assuming the maximum possible direct feeding (11%) to the ground state. This is consistent with a first forbidden decay. Conversely, if the β decay is first forbidden unique, as required if the ^{40}P ground state is 2^-, then we could estimate an upper limit on the ground state feeding, using a log(ft) of 8, of 0.13% that would be consistent with no feeding given the limits of this experiment. We, therefore, assume that the feeding to the ^{40}S ground state is negligible, and the unobserved feeding must go to other states. The second possibility is that the missing feeding is related to unidentified levels populated in the decay. In the experiment, γ-ray spectra were only collected up to 4.2 MeV. This leaves a significant window for feeding to additional bound states below the neutron separation energy at 7.65 MeV [30]. Any transitions from these states to the ground state or the first three excited states would have been missed. Given the pattern for the γ decays observed, i.e., strong transitions to the 903-keV state, one might expect a similar pattern for higher lying states. The fact that no escape peaks, i.e., unplaced γ rays, are observed for strong γ rays with energies greater than 4.2 MeV may indicate that the feeding to these states is weak. The effect of additional states is still limited unless the states decay directly to the ground state. For example, if a γ ray feeds the 903-keV level then it reduces feeding to this level but adds the same amount into the missing level. Hence, there will be no effect on the overall determination of the missing feeding. All log(ft) values obtained here are probably lower limits since some of the decay strength may be shifted to higher energy states.

TABLE III. Level energies in ^{40}S populated in the β decay of ^{40}P.

Energy (keV)	Feeding(%)[a]	log(ft)[b]
903.69$\pm$0.07	9.6$\pm$2.7	6.08$\pm$0.13
1916.84$\pm$0.21		
2254.79$\pm$0.12	1.6$\pm$0.9	6.64$\pm$0.25
3236.1$\pm$0.3	0.7$\pm$0.3	6.82$\pm$0.20
3489.46$\pm$0.18	14.1$\pm$1.8	5.47$\pm$0.08
3947.0$\pm$0.3	3.4$\pm$0.5	6.00$\pm$0.09
4138.30$\pm$0.20	29.8$\pm$2.6	5.02$\pm$0.08
4724.61$\pm$0.23	7.5$\pm$1.2	5.60$\pm$0.10
5009.4$\pm$0.4	11.3$\pm$1.6	5.26$\pm$0.09

[a]Based on measured absolute feeding of the 903-keV γ ray.
[b]Based on $Q_\beta=14.5\pm0.3$ MeV [31].

Using the absolute feedings as describe previously, log(ft) values for each of the observed states were determined and are presented in Table III. The log(ft) value of 6.08 for the first excited state is consistent with a first forbidden decay. This result coupled with the theoretical arguments presented previously limits the spin/parity for the ^{40}P ground state to $(2,3)^-$. The strong feeding and low log(ft) values of the decay to the states at 3489, 4138, and 5009 keV are consistent with allowed decays indicating that these states are most likely odd parity states. Each has a strong transition to the 903-keV 2_1^+ state, while the 3489-keV state also has a strong transition to the ground state. This strong ground-state transition indicates the 3489-keV state must have a low spin with the possible spin/parity assignments being $1^\pm$ or 2^+. In addition, the ratio of transition intensities between the 2585-

and 3489-keV transitions suggests that the two have the same multipolarity, probably $E1$, with the 2585-keV transition being more hindered. If the multipolarity of these γ rays is $E1$, then the 3489-keV state has a spin/parity of 1^- that would limit the ground state of ^{40}P to 2^-. However, it is not possible to rule out a first forbidden β decay to the 3489-keV state that would then yield, when considering the 2585- to 3489-keV intensity ratio, a spin/parity of $(1,2)^+$ for this state. Hence, additional evidence is needed to differentiate the spin/parity for the ^{40}P ground state between 2^- and 3^-. A direct measurement of the multipolarity of the 3489-keV transition would clarify this assignment.

E. Level Structure of ^{40}S

The low-energy levels in ^{40}S observed in ^{40}P β decay are presented in Fig. 4. The first excited state at 903 keV is consistent with the energy obtained by Scheit *et al.* that supports the assignment of this state as 2^+ [8]. Except for the 3489-keV transition, the decay of all other excited states lack strong ground-state transitions and pass through the 903-keV state. This suggests that the states populated in the decay are primarily of spin 2 or higher.

The second and third states, at 1916 and 2254 keV, respectively, exhibit little or no feeding in the β decay. Nuclear structure considerations suggest that these two states are part of the vibrational two-phonon triplet. This assumption is supported by the fact that each state decays primarily to the 2_1^+ state. The weak 2254-keV γ ray has a large sum peak component although some of the intensity can come from an actual transition. However, this transition is significantly hindered relative to the 1351-keV transition. In considering β decay to these states, only first forbidden decay should be observed since first forbidden unique or higher order forbidden decays will be too weak to be observed in our data. The log(ft) value for the 2254-keV state is consistent with a first forbidden decay that along with observation of the 2254-keV γ ray suggests that this state is the 2^+ member of the triplet. The state at 1916 keV could be either the 0^+ or 4^+ member of the triplet, but the expectation that mainly higher spin states are being populated points more strongly to this being the 4^+ state. A precise assignment of spin/parity is not possible with the current data, but the range of values for the ratio $E_{4_1^+}/E_{2_1^+}$ is 2.12 to 2.50 indicating predominately vibrational structure.

As mentioned previously, the states at 3489, 4138, and 5009 keV are all strongly fed and have log(ft) values that are consistent with allowed decays. This would limit the spin/parity for each state to $(1,2,3,4)^-$. Consideration of the transitions from the 3489-keV state suggests the most probable spin/parity assignment to be 1^-. However, since a first forbidden decay is not disallowed, a spin/parity assignment of 1^+ or 2^+ is also possible. For the other three states, the lack of a ground state transition rules out a 1^- assignment. For the 4138-keV state, which has the strongest feeding in the decay, the transitions to the 903- and 3489-keV states have an intensity ratio that differs significantly from the Weisskopf estimates. For example, if the 3489-keV state has a 1^- spin/parity and the 4138-keV state has a spin/parity of 2^- then the two transitions are $E1$ and $M1$, respectively. This assumption indicates that the 648-keV transition is enhanced relative to the 3234-keV transition by a factor of 400 in comparison to the Weisskopf estimate. A closer value is obtained if the 3489-keV state is 1^+ or 2^+ in which case both transitions are $E1$ and the relative enhancement of the 648-keV transition, or hinderance of the 3235-keV transition, is only 20 times greater than the Weisskopf estimate. Both of these situations are possible and detailed measurements on the 648- and 3234-keV transitions would provide significant information about the structure of this nucleus.

The states at 3236 and 3947 keV are both weakly fed in the decay and have log(ft) values consistent with first forbidden decays. As such, they are most likely even parity states which could be part of the three-phonon vibrational states. However, the 3043-keV transition from the 3947-keV state is inconsistent with this assumption. Therefore, at least for the 3947-keV state, a more complicated structure is present. The 4724-keV state has a log(ft) value that is consistent with either allowed or first forbidden decay. The fact that it decays only to members of the two-phonon triplet suggests that it is probably an even parity state and also may be part of the three-phonon multiplet.

IV. COMPARISONS

A comparison of the low-energy structure of ^{40}S can easily be made to the adjacent even-even nuclide ^{42}Ar since it differs only by the addition of two protons into the sd shell placing it is closer to a closed proton shell while remaining midshell for neutrons. The low-energy structure of ^{42}Ar has been measured using the ^{40}Ar(t,p) and ^{40}Ar($t,p\gamma$) reactions [34–37], through ^{42}Cl β decay [38], and by direct proton scattering [17]. These experiments have resulted in a detailed level scheme with states up to 7.6 MeV. The quadrupole deformation parameter ($|\beta_2|$) for the 2_1^+ state has been determined by nuclear lifetime measurements (0.26 ± 0.03 [36]) and proton scattering (0.32 ± 0.05 [17]) for ^{42}Ar, and by Coulomb Excitation (0.284 ± 0.016 [8]) and proton scattering (0.35 ± 0.05 [15]) for ^{40}S. The similarity of these results suggest that the basic structure should be similar. Fig. 6 provides a comparison of the states in ^{42}Ar and ^{40}S up to $\sim$3.5 MeV.

The low-energy structure for ^{42}Ar is that expected for a nearly pure harmonic vibrational nucleus up to 3.0 MeV with additional structures becoming more dominant at higher energies. The strong hindrance of the 2_2^+ to ground state transition indicates that the admixture with nonvibrational states is not significant for the one- and two-phonon excitations. However, the observation of states near 3.0 MeV that are not members of the three-phonon excitation indicate that the structure becomes dominated by other effects at this energy. By comparison, the low-energy structure of ^{40}S has the characteristics of an anharmonic vibrational nucleus up to 3.0 MeV since the energy of the 2_1^+ state is depressed, the energy separation between the expected two-phonon states is increased, and the average energy of the two-phonon states is more than twice that of the 2_1^+ state. Although the energy of the first excited state is depressed, it is still at a relatively

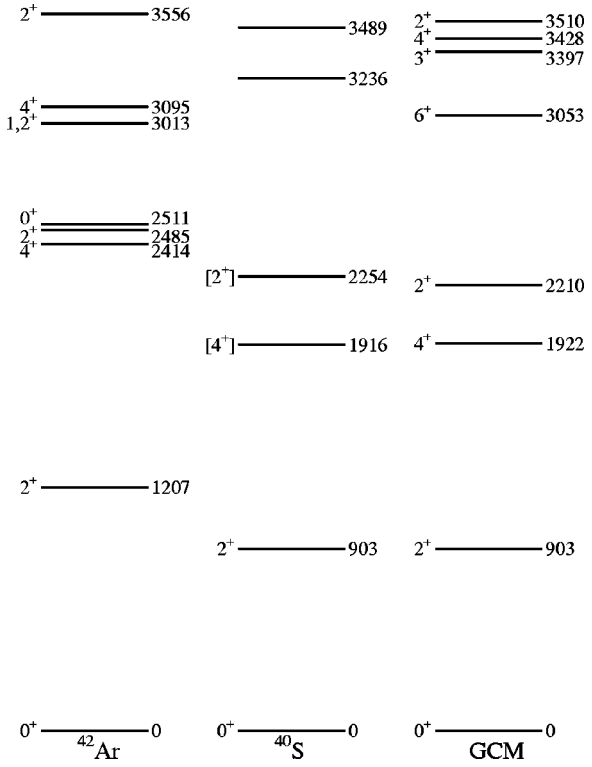

FIG. 6. Comparison of the level scheme for ^{40}S to the level scheme for ^{42}Ar and the results of a GCM calculation. See text for details.

high energy compared to what would be expected for a strongly deformed nucleus showing rotational collectivity. The 2_2^+ to ground state transition (2254-keV γ ray) is strongly hindered indicating that at least for the lowest states the admixture from other structures is minimal. Although the 1916 keV state could be either the 0_2^+ or 4_1^+ state, the similarity to ^{42}Ar suggests that the latter assignment is more likely. This indicates an $E(4_1^+)/E(2_1^+)$ ratio of 2.12 that one might expect for a nucleus with a small amount of deformation.

A comparison has also been made to model calculation results using the Geometrical Collective Model (GCM) [39–41]. The GCM is based upon a solution of the Bohr Hamiltonian for a potential $V(\beta,\gamma)$, expanded in powers of β and $\cos 3\gamma$, and so analysis using the GCM provides insight into the shape of the nuclear potential. In particular, since the level scheme for ^{40}S is consistent with that of an anharmonic vibrator, it is interesting to estimate the anharmonicity of the potential. The parameters for the calculation were chosen to reproduce the energies of the levels at 903, 1916, and 2254 keV and the $B(E2;0_{\text{g.s.}}^+ \rightarrow 2_1^+)$ value of 334 ± 36 $e^2\text{fm}^4$ [8]. In view of the small number of experimental observables available for determining the parameters, it is important to limit the number of free parameters in the model, and so a restricted potential [42]

$$V(\beta,\gamma) = C_2 \frac{1}{\sqrt{5}}\beta^2 - C_3\sqrt{\frac{2}{35}}\beta^3 \cos 3\gamma + C_4 \frac{1}{5}\beta^4$$

was used. The Hamiltonian also contains a mass parameter B_2 in the kinetic-energy operator.

The results of this calculation are shown in Fig. 6. The parameter values obtained are $B_2 = 12.6 \times 10^{-42}$ MeV s^2, $C_2 = -18.3$ MeV, $C_3 = 96.7$ MeV, and $C_4 = 460$ MeV. These parameters correspond to a β-soft potential with a shallow oblate minimum and a somewhat deeper prolate minimum. However, the depths of these minima are small compared to the zero-point energy of the ground state, and so the nucleus sees essentially an oscillator-like but anharmonic potential.

The closely spaced levels at 1916 and 2254 keV are suggestive of the degenerate $2^+/4^+$ pair of levels which occurs for γ-independent potentials [43] ($C_3 = 0$). Introduction of a γ dependence through a nonzero C_3 term, to reproduce the observed splitting of the 2^+ and 4^+ levels, inevitably lowers the 4^+ state and raises the 2^+. Therefore, good agreement with experiment can be obtained only if the 1916-keV level is assigned as the 4_1^+ state, as was suggested above in the comparison to ^{42}Ar. The GCM calculations additionally predict a 0^+ level at approximately the same energy as the 4^+ level, but such a level would not necessarily be strongly populated in this β decay due to its low spin. The observed level at 3236 keV may be identified with the 2_3^+, 3_1^+, or 4_2^+ levels in the GCM calculation. All three of these levels in the model calculations decay with large $B(E2)$ strengths to the 4_1^+ and 2_2^+ levels but only weakly to the 0_1^+ or 2_1^+ states, with $B(E2)$ strengths suppressed by roughly two orders of magnitude.

V. CONCLUSIONS

In this paper we have presented results on the β decay properties of ^{40}P that was produced by the fragmentation of a ^{48}Ca beam. The half-life of ^{40}P was measured to be 153 ± 8 ms while the delayed-neutron probability was found to be $15.8 \pm 2.1\%$, both of which differ significantly from previous measurements. A total of 15 γ rays were assigned to the β branch that fed nine levels in the daughter nucleus ^{40}S, while three γ rays are assigned to the β-n branch based on the results of a separate experiment which observed the β decay of ^{39}P [25]. 60% of the feeding is to four states above 3.0 MeV. The low log(ft) values indicate allowed transitions to negative parity states which would consist primarily of coupled shell model states. The observed levels for ^{40}S at low energy are consistent with that of an anharmonic vibrator. A GCM calculation with parameters fit to the experimentally measured level energies and $B(E2,0_{\text{g.s.}}^+ \rightarrow 2_1^+)$ value indicate a soft and shallow potential with a deeper prolate minimum. Whereas the Coulomb excitation measurements provide the magnitude of the β_2 value [8], use of β decay to determine the location of the 4_1^+ state at 1916 keV makes it is possible to determine the sign of β_2 as positive.

ACKNOWLEDGMENTS

This work was supported by the U.S. Department of Energy under Contract Nos. DE-FG02-96ER-41006 and DE-FG02-91ER-40609, and by the National Science Foundation under Contract No. PHY-95-28844.

[1] H. Sakurai, S.M. Lukyanov, M. Notani, N. Aoi, D. Beaumel, N. Fukuda, M. Hirai, E. Ideguchi, N. Imai, M. Ishihara, H. Iwasaki, T. Kubo, K. Kusaka, H. Kumagai, T. Nakamura, H. Ogawa, Yu.E. Penionzhkevich, T. Teranishi, Y.X. Watanabe, K. Yoneda, and A. Yoshida, Phys. Lett. B **448**, 180 (1999).

[2] Z. Dlouhý, Yu. Penionzhkevich, R. Anne, D. Baiborodin, C. Borcea, A. Formichev, D. Guillemaud-Mueller, R. Kalpakchieva, M. Lewitowicz, S. Lukyanov, A.C. Muller, Yu. Oganessian, R.D. Page, A. Ree, M.G. Saint-Laurent, E. Sokol, N. Skobelev, O. Sorlin, O. Tarasov, V. Toneev, and W. Trinder, J. Phys. G **25**, 859 (1999).

[3] P. Möller and J.R. Nix, At. Data Nucl. Data Tables **26**, 165 (1981).

[4] T.R. Werner, J.A. Sheikh, W. Nazarewicz, M.R. Strayer, A.S. Umar, and M. Misu, Phys. Lett. B **333**, 303 (1994); **335**, 259 (1994).

[5] T.R. Werner, J.A. Sheikh, M. Misu, W. Nazarewicz, J. Rikovska, K. Heeger, A.S. Umar, and M.R. Strayer, Nucl. Phys. **A957**, 327 (1996).

[6] O. Sorlin, D. Guillemaud-Mueller, A.C. Mueller, V. Borrel, S. Dogny, F. Pougheon, K.-L. Kratz, H. Gabelmann, B. Pfeiffer, A. Wöhr, W. Ziegert, Yu.E. Penionzhkevich, S.M. Lukyanov, V.S. Salamatin, R. Anne, C. Borcea, L.K. Fifield, M. Lewitowicz, M.G. Saint-Laurent, D. Bazin, C. Détraz, F.-K. Thieleman, and W. Hillebrandt, Phys. Rev. C **47**, 2941 (1993).

[7] O. Sorlin, D. Guillemaud-Mueller, R. Anne, L. Axelsson, D. Bazin, W. Böhmer, V. Borrel, Y. Jading, H. Keller, K.-L. Kratz, M. Lewitowicz, S.M. Lukyanov, T. Mehren, A.C. Mueller, Yu.E. Penionzhkevich, F. Pougheon, M.G. Saint-Laurent, V.S. Salamatin, S. Shoedder, and A. Wöhr, Nucl. Phys. **A583**, 763 (1995).

[8] H. Scheit, T. Glasmacher, B.A. Brown, J.A. Brown, P.D. Cottle, P.G. Hansen, R. Harkewicz, M. Hellstrom, R.W. Ibbotson, J.K. Jewell, K.W. Kemper, D.J. Morrissey, M. Steiner, P. Thirolf, and M. Thoennessen, Phys. Rev. Lett. **77**, 3967 (1996).

[9] T. Glasmacher, B.A. Brown, J.J. Chromik, P.D. Cottle, M. Fauerbach, R.W. Ibbotson, K.W. Kemper, D.J. Morrissey, H. Scheit, D.W. Sklenicka, and M. Steiner, Phys. Lett. B **395**, 163 (1997).

[10] T. Glasmacher, Nucl. Phys. **A630**, 278c (1998).

[11] R.W. Ibbotson, T. Glasmacher, B.A. Brown, L. Chen, M.J. Chromik, P.D. Cottle, M. Fauerbach, K.W. Kemper, D.J. Morrissey, H. Scheit, and M. Thoennessen, Phys. Rev. Lett. **80**, 2081 (1998).

[12] R.W. Ibbotson, T. Glasmacher, P.F. Mantica, and H. Scheit, Phys. Rev. C **59**, 642 (1999).

[13] A.M. Bernstein, V.R. Brown and V.A. Madsen, Phys. Lett. **103B**, 255 (1981).

[14] J.H. Kelley, T. Suomijärvi, S.E. Hirzebruch, A. Azhari, D. Bazin, Y. Blumenfeld, J.A. Brown, P.D. Cottle, S. Danczyk, M. Fauerbach, T. Glasmacher, J.K. Jewell, K.W. Kemper, F. Maréchal, D.J. Morrissey, S. Ottini, J.A. Scapaci, and P. Thirolf, Phys. Rev. C **56**, R1206 (1997).

[15] F. Maréchal, T. Suomijärvi, Y. Blumenfeld, A. Azhari, E. Bauge, D. Bazin, J.A. Brown, P.D. Cottle, J.P. Delaroche, M. Fauerbach, M. Girod, T. Glasmacher, S.E. Hirzebruch, J.K. Jewell, J.H. Kelley, K.W. Kemper, P.F. Mantica, D.J. Morrissey, L.A. Riley, J.A. Scarpaci, H. Scheit, and M. Steiner, Phys. Rev. C **60**, 034615 (1999).

[16] F. Maréchal, T. Suomijärvi, Y. Blumenfeld, A. Azhari, D. Bazin, J.A. Brown, P.D. Cottle, M. Fauerbach, T. Glasmacher, S.E. Hirzebruch, J.K. Jewell, J.H. Kelley, K.W. Kemper, P.F. Mantica, D.J. Morrissey, L.A. Riley, J.A. Scarpaci, H. Scheit, and M. Steiner, Phys. Rev. C **60**, 064623 (1999).

[17] H. Scheit, F. Maréchal, T. Glasmacher, E. Bauge, Y. Blumenfeld, J.P. Delaroche, M. Girod, R.W. Ibbotson, K.W. Kemper, J. Libert, B. Pritychenko, and T. Suomijarvi, Phys. Rev. C **63**, 014604 (2001).

[18] J.P. Dufour, R. Del Moral, A. Fleury, F. Hubert, D. Jean, M.S. Pravikoff, H. Delagrange, H. Geissel, and K.-H. Schmidt, Z. Phys. A **324**, 487 (1986).

[19] M. Lewitowicz, Yu.E. Penionzhkevich, A.G. Artukh, A.M. Kalinin, V.V. Kamanin, S.M. Luyanov, N.H. Chau, A.C. Mueller, D. Guillemaud-Mueller, R. Anne, D. Bazin, C. Détraz, D. Guerreau, M.G. Saint-Laurent, V. Borrel, J.C. Jacmart, F. Pougheon, A. Richard, and W.D. Schmidt-Ott, Nucl. Phys. **A496**, 477 (1989).

[20] B.M. Sherrill, D.J. Morrissey, J.A. Nolen, Jr., and J.A. Winger, Nucl. Instrum. Methods Phys. Res. B **56/57**, 1106 (1991).

[21] R. Harkewicz, Rev. Sci. Instrum. **67**, 2176 (1996).

[22] G.F. Knoll, *Radiation Detection and Measurement* (Wiley, New York, 1989), p. 435.

[23] A. Owens, Nucl. Instrum. Methods Phys. Res. A **274**, 297 (1989).

[24] Z. Kis, B. Fazekas, J. Östör, Zs. Révay, T. Belgya, G.L. Molnár, and L. Koltay, Nucl. Instrum. Methods Phys. Res. A **418**, 374 (1998).

[25] J.A. Winger, H.H. Yousif, W.C. Ma, V. Ravikumar, W. Lui, S.K. Phillips, R.B. Piercey, P.F. Mantica, B. Pritychenko, R.M. Ronningen, and M. Steiner, in *ENAM 98*, *Exotic Nuclei and Atomic Masses*, edited by B.M. Sherrill, D.J. Morrissey, and C.N. Davids, AIP Conf. Proc. No. 455 (AIP, Woodbury, NY, 1998).

[26] K. Takahashi, M. Yamada, and T. Kondoh, At. Data Nucl. Data Tables **12**, 101 (1973).

[27] H. Nakata, T. Tachibana, and M. Yamada, Nucl. Phys. **A594**, 27 (1995).

[28] H.V. Klapdor, J. Metzinger, and T. Oda, At. Data Nucl. Data Tables **31**, 81 (1984).

[29] A. Staudt, E. Bender, K. Muto, and H.V. Klapdor-Kleingrothaus, At. Data Nucl. Data Tables **44**, 79 (1990).

[30] P. Möller, J.R. Nix, and K.-L. Kratz, At. Data Nucl. Data Tables **66**, 131 (1997).

[31] X.G. Zhou, X.L. Tu, J.M. Wouters, D.J. Vieira, K.E.G. Lobner, H.L. Seifert, Z.Y. Zhou, and G.W. Butler, Phys. Lett. B **260**, 285 (1991).

[32] John C. Hill, R.F. Petry, and K.H. Wang, Phys. Rev. C **21**, 384 (1980).

[33] G. Klotz, J.P. Gonidec, P. Baumann, and G. Walter, Nucl. Phys. **A197**, 229 (1972).

[34] R.F. Casten, E.R. Flynn, J.D. Garrett, S. Orbesen, and O. Hansen, Phys. Lett. **43B**, 473 (1973).

[35] J.G. Pronko and R.E. McDonald, Phys. Rev. C **7**, 1061 (1973).

[36] T.R. Fisher, T.T. Bardin, J.A. Becker, and B.A. Watson, Phys. Rev. C **9**, 598 (1974).

[37] E.R. Flynn, O. Hansen, R.F. Casten, J.D. Garrett, and F.

Ajzenberg-Selove, Nucl. Phys. **A246**, 117 (1975).
[38] A. Huck *et al.*, in *Proceedings of the 4th International Conference on Nuclei Far from Stability*, edited by L. O. Skolen (Helsingor, Denmark, 1981), Vol. 2, p. 378.
[39] G. Gneuss, U. Mosel, and W. Greiner, Phys. Lett. **30B**, 397 (1969).
[40] G. Gneuss and W. Greiner, Nucl. Phys. **A171**, 449 (1971).
[41] D. Troltenier, J.A. Maruhn, and P.O. Hess, in *Computational Nuclear Physics*, edited by K. Langanke, J.A. Maruhn, and S.E. Koonin (Springer, Berlin, 1991), p. 105.
[42] J.-Y. Zhang, R.F. Casten, and N.V. Zamfir, Phys. Lett. B **407**, 201 (1997).
[43] L. Wilets and M. Jean, Phys. Rev. **102**, 788 (1956).